

CurviTrack: Curvilinear Trajectory Tracking for High-speed Chase of a USV

Parakh M. Gupta, Ondřej Procházka, Tiago Nascimento, *Senior Member, IEEE*, and Martin Saska *Member, IEEE*

Abstract—Heterogeneous robot teams used in marine environments incur time-and-energy penalties when the marine vehicle has to halt the mission to allow the autonomous aerial vehicle to land for recharging. In this paper, we present a solution for this problem using a novel drag-aware model formulation which is coupled with Model Predictive Control (MPC), and therefore, enables tracking and landing during high-speed curvilinear trajectories of an Unmanned Surface Vehicle (USV) without any communication. Compared to the state-of-the-art, our approach yields 40% decrease in prediction errors, and provides a 3-fold increase in certainty of predictions. Consequently, this leads to a 30% improvement in tracking performance and 40% higher success in landing on a moving USV even during aggressive turns that are unfeasible for conventional marine missions. We test our approach in two different real-world scenarios with marine vessels of two different sizes and further solidify our results through statistical analysis in simulation to demonstrate the robustness of our method.

Index Terms—Aerial Systems: Mechanics and Control, UAV, MPC, Optimization and Optimal Control, Multi-Robot Systems, Dynamics

URL: <https://mrs.fel.cvut.cz/curvitrac-boat-landing>

I. INTRODUCTION

THE increased demand for exploring, maintaining, and studying the vast open-water habitats of our planet has created a pressing need for a cost-effective unmanned system that can accomplish these tasks autonomously and efficiently. Exploration requires a high vantage point and agility which are primary strengths of an Unmanned Aerial Vehicle (UAV), but UAVs suffer from small payload capabilities and limited flight times. Conversely, USVs can carry higher payloads and conduct long-range missions due to their higher battery capacity. They can also be equipped with more sensors for localisation, water and air sampling, and sea-floor mapping. Therefore, a heterogeneous team of aerial and marine vehicles

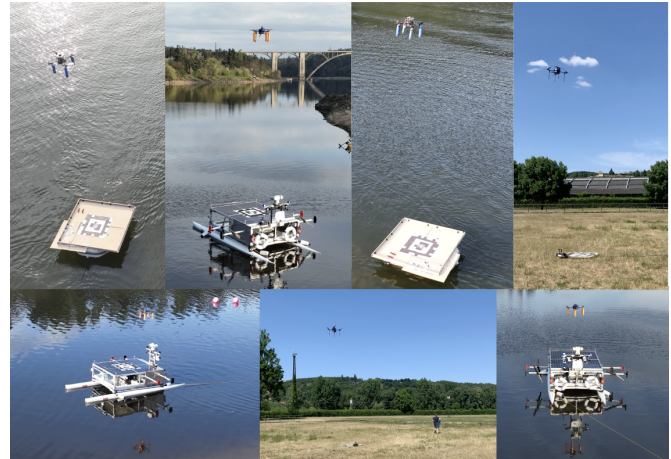


Fig. 1: A collage of various moments from the real-world experiments.

can accomplish tasks pertaining to exploration, infrastructure maintenance, port security, search-and-rescue, surveillance, and ocean cleanup with greater efficiency than each of the vehicles by itself. Murphy et al. [1] demonstrated how they used a UAV and a USV to assess structural damages caused by hurricane Wilma. Building on these insights, Lindemuth et al. [2] presented a UAV-USV team where the USV served as an interface between underwater and surface operations while the UAV provided assistance through better localisation and by acting as a communication relay. As demonstrated by Ramirez et al. [3], the UAV can also aid in open waters from its vantage point by predicting the drift of a lost person using wind and sea currents, and by informing the USV so it can perform the final rescue. In these applications, current UAV designs are limited by their battery lives and hence, the capability to autonomously land and recharge on mobile platforms in marine environments emerges as a pivotal and essential technology for a seamless and completely autonomous operation.

One of the challenges during such a landing manoeuvre is that a tilted landing deck can result in the UAV rolling or sliding off the platform, which, in turn, can trigger unintended responses from the controller of the UAV, and thus, lead to disastrous consequences. Additionally, a vertically oscillating deck can transfer significant impulse into the aircraft in case of vertical velocity mismatch and wreak havoc on its fuselage during landing. Predicting such motion can alleviate these issues; Riola et al. [4] and Kuchler et al. [5] demonstrated that past measurements of the periodic ship motion, resulting from waves, can be used to forecast future behaviour with a fair de-

Manuscript received: October 9th, 2024; Revised January 7th, 2025; Accepted February 15th, 2025.

This paper was recommended for publication by Editor Giuseppe Loianno upon evaluation of the Associate Editor and Reviewers' comments.

This work has been supported by CTU grant no SGS23/177/OHK3/3T/13, by the Czech Science Foundation (GAČR) under research project No. 23-06162M, by the European Union under the project Robotics and advanced industrial production (reg. no. CZ.02.01.01/00/22_008/0004590), and by the National Council for Scientific and Technological Development – CNPq from Brazil under research project No. 304551/2023-6 and 407334/2022-0.

P. M. Gupta, O. Procházka, T. Nascimento, and M. Saska are with the Department of Cybernetics, Czech Technical University in Prague, Prague, Czech Republic (e-mail: guptapar@fel.cvut.cz, see <https://mrs.fel.cvut.cz/curvitrac-boat-landing>)

T. Nascimento is also with the Department of Computer Systems, Universidade Federal da Paraíba, Brazil

Digital Object Identifier (DOI): see top of this page.

gree of accuracy for short prediction horizons. Landing during this wave-induced periodic motion was previously addressed in our work on landing a UAV in harsh winds and turbulent open-waters [6]. However, as mentioned in [6], it was observed that significant time was lost in the motion estimation, and the USV had to be stationary for this duration instead of conducting the manoeuvres necessary for the completion of its mission. These missions usually require sweeping scans, in parallel track patterns [7], which requires constant turning of the USV; therefore, a landing solution limited to the scope of straight-line motion does not aid in the recovery of lost efficiency. Obtaining information about the USV is another challenge in the open waters. Similarly to our previous work, our proposed approach is dedicated to constructing a versatile decentralized solution independent of direct communication, as communication infrastructure in the open waters may not reliably fulfill the stringent localisation requirements such as high frame rates and low latency. Therefore, in this article, we expand our previous work to focus on tracking and landing during deliberate translational motion of the USV and propose a new approach to predict the linear and curvilinear motion in x and y axis of the USV (figure 3) at high speeds; we rely on the prediction of periodic oscillation of the USV in z axis (heave) from our previous work [6] to ensure that the touchdown velocity during landing is minimised, and the UAV lands with minimal impulse transfer.

II. RELATED WORKS

Landing on a slowly oscillating marine vessel has been a keenly studied area of research in the recent past. One of the pioneering efforts in this domain was undertaken by Polvara et al. [8], who introduced a methodology employing a fiducial marker positioned on the platform, and leveraged an Extended Kalman Filter (EKF) to estimate the position of the USV. In contrast, Abujoub et al. [9] adopted a different strategy by utilizing a Light Detection and Ranging (LiDAR) system onboard the UAV to ascertain the pose of the landing pad. Similarly, Yang et al. [10] presented an approach for image-based visual servoing (IBVS) tailored for a UAV aiming to execute a successful landing onto a boat using a downward-facing camera.

However, fewer works are available that focus on landing on a moving USV and the majority of these focus on straight-line paths for a general platform. Herissé et al. [11] presented one of the first investigations for landing on a general moving platform using optical flow to handle lateral velocities. However, the authors do not consider any predictive model of the underlying vehicle, and therefore, the success of the landing is contingent on the constraints matching between the UAV and the landing platform. Such an approach would be infeasible for a rapidly turning USV. Cengiz et al. [12] present an investigation into the feasibility of implementing two optimal control approaches to enable a quadrotor to autonomously track and follow a mobile platform, commencing from an arbitrary initial position and ultimately executing a precision landing on the said platform. The study demonstrated the superiority of the MPC but did not elaborate on the modelling

of the USV. In contrast, Zhao et al. [13] proposed a visual servoing approach and validated their experiments using real robots, but for a general moving target unlike a marine vessel, and without consideration of the model of the moving platform. Falanga et al. [14] expanded the state-of-the-art by increasing the velocity of the UAV up to 1.5 m s^{-1} , but only in straight lines and following a ground robot. The tracking speed record was presented in the work of Borowczyk et al. [15], where the authors successfully reached a speed of 13.8 m s^{-1} in real-world experiments for straight-line motion and assumed communication between the two robots.

The work of Lee et al. [16] demonstrated a PID-based approach in a simulated environment that achieved high tracking speeds of up to 8 m s^{-1} in a straight line. Their approach does not consider the model of the platform and instead relies on matching constraints between the UAV and the landing platform. They also show S-curves of slow speed in simulation, but their real-world results are presented for slow linear motion. Baca et al. [17] presented one of the first modelling-based approaches with real-world experiments that show the UAV landing on a moving ground vehicle for a curved track without any communication. However, the trajectory of the ground vehicle was known a priori, enabling the authors to bias the predictions to the expected curved track.

Novák et al. [18] presented the current state-of-the-art in modelling and predicting the motion of a USV using a sophisticated model that considers the hydrodynamic, hydro-static, and Coriolis forces acting on the USV. They also leverage communication between the vehicles to obtain information from the sensor stack onboard the USV to improve state-estimation of the UAV by localising in relation to the USV frame. This model is deployed inside an Unscented Kalman Filter (UKF), along with a simplified model deployed in a Linear Kalman Filter (LKF) for comparison, and both the models rely on multiple sensors and communicated states for state estimation to obtain pose and velocities of the USV. However, the stated requirements of various states and their derivatives lead to poor convergence for challenging turns and curvilinear trajectories, especially when sufficient sensory information cannot be provided without communicating. Procházka et al. [19] use the estimator presented in [18] to track and land on the marine vessel at low speeds through curvilinear trajectories. However, after careful review, it was found that none of the discussed approaches converge well for high-speed curvilinear trajectories, and perform poorly on communicated-denied scenarios due to model complexity. Both of these drawbacks are detrimental in agile missions of closely cooperating heterogeneous UAV-USV teams in real-world conditions and are, therefore, the primary focus of our presented work in this paper. To this end, we propose a novel decentralized modelling approach which converges reliably on limited information from visual pose estimation, and predicts the curvilinear motion of the USV for performing high-speed tracking and landing on the USV. Despite these drawbacks, we found that [18] was most suited for the comparison and therefore, we present a comparison through statistical analysis in simulation, and bolster our claims by testing our novel approach in several real-world scenarios. In summary, our

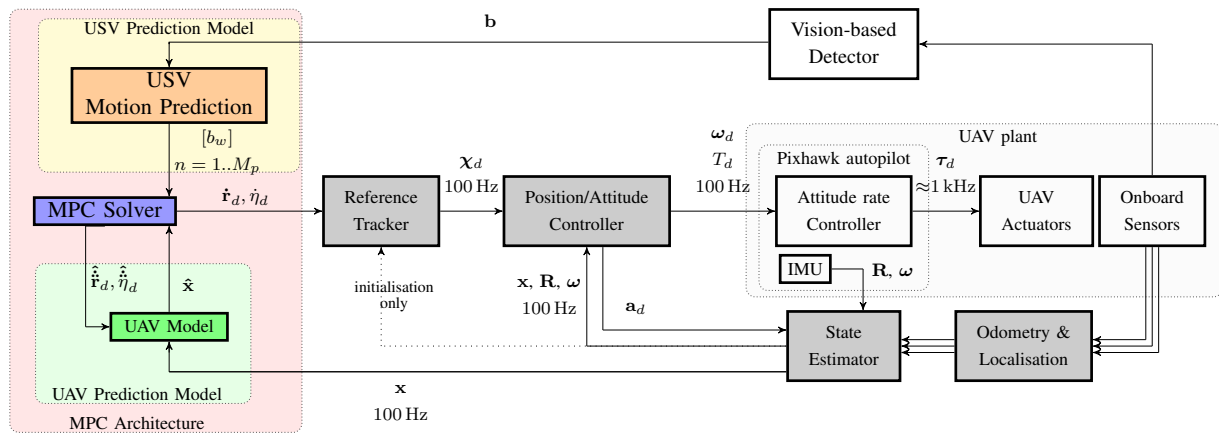


Fig. 2: The entire UAV control architecture; the *MPC* landing controller (red block) is integrated into the *MRS* system [20] (grey blocks) and supplies the desired reference (velocity $\dot{\mathbf{r}}_d = [\dot{x} \ \dot{y} \ \dot{z}]^T$ and heading rate $\dot{\eta}_d$). In the *MRS* system, the first layer containing a *Reference tracker* processes the desired reference and gives a full-state reference χ to the attitude controller. The feedback *Position/Attitude controller* produces the desired thrust and angular velocities (T_d, ω_d) for the Pixhawk flight controller (*Attitude rate controller*). The *State estimator* fuses data from *Odometry & localisation* methods to create an estimate of the UAV translation and rotation (\mathbf{x}, \mathbf{R}) . The *Vision-based Detector* obtains the visual data from the camera and sends the pose information \mathbf{b} of the USV to the *MPC*. The individual states are sent to their respective prediction models, and using these predictions, the *MPC* generates the desired control reference according to the cost function.

contributions are:

- a novel drag-aware linear model inside an LKF to predict the future curvilinear motion of a USV using only visual pose estimation, and
- an MPC based control approach for following a high-speed USV during curvilinear trajectories, and for landing with minimal impulse transfer.

A supplementary video of the experiments is attached to this paper and can also be found at <https://mrs.fel.cvut.cz/curvitrack-boat-landing>.

III. HIGH-SPEED CHASE AND LANDING APPROACH

In this section, we propose our model-based method for predicting, tracking, and landing using two separate models for the USV and the UAV. The UAV model is embedded inside the MPC and is used to make predictions about the state of the UAV for control. Similar to our previous work [6], our proposed controller receives the predicted states of the USV as an input reference and must produce a control reference at a minimum of 20 Hz, within the constraints of the mission (max velocity, max acceleration, and max jerk). The MPC produces control outputs, for desired linear velocities and the desired heading rate of the UAV, which are sent to the underlying *MRS*-system [20] framework as described in figure 2.

For the USV model, we formulate a linear Kalman estimator with a point-mass model and include the velocity states as observed variables while the pose of the USV remains a measured variable. This model, on its own, works sufficiently well for straight-line motion with low-acceleration constraints, and does not require input generation. When this model is deployed for curving paths, the predicted path is a straight line tangential to the current curvature of the path, as shown

in figure 3. So, to perform predictions about the turning of the USV, we introduce a method of generating the input to the model using drag simulations that cause the predicted paths to curve due to centripetal acceleration. Compared to the state-of-the-art, another important aspect of our novel method is the ability to account for the negative covariance between the velocity of the USV and its yaw rate. In summary, this novel approach solves the limitations of our previous USV model in [6] and, for the first time, enables tracking during curvilinear motion, even at speeds of up to 5 m s^{-1} . Finally, we highlight that the proposed model is specifically demonstrated for systems that operate on information limited to pose and are required to make predictions about the future motion of the USV with no communication. However, the proposed technique is not limited by the chosen perception and sensor setup, and direct access to velocity and acceleration states of the USV (either through communication or a different sensor) can be used to improve the tracking performance, to decrease the filter convergence time, and to expand the mission operation envelope. For example, direct access to Inertial Measurement Unit (IMU) information can help lift the low-acceleration constraints and improve the angular and translational velocity estimation errors. Since this information is difficult to obtain in the real world, and relative localisation techniques are well-developed and often chosen in missions, we limit our scope to the use of pose information for the USV to demonstrate the robustness of our approach.

A. USV Prediction Model

For a USV moving through a fluid, form drag (also called pressure drag) is the primary factor affecting the curvilinear motion. Therefore, we simulate the form drag experienced by

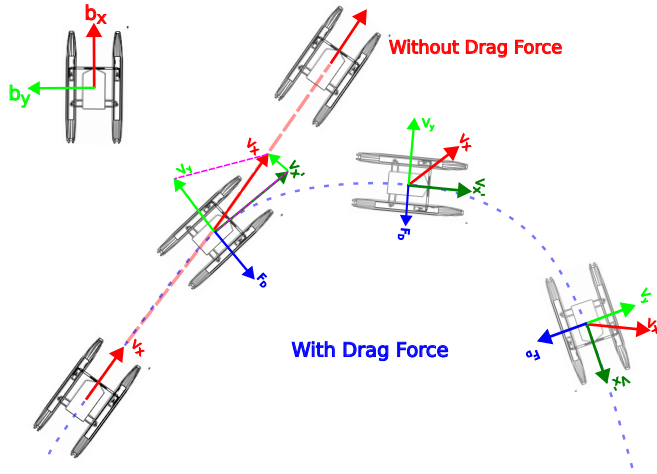


Fig. 3: The red path represents the unchanged path taken by the USV when no drag force is acting on it; whereas the blue path shows how the difference between V_x and V_x' produces a V_y vector and therefore, causes significant drag that leads to the turning of the USV.

the vessel to generate inputs to a Kalman filter, which causes the predictions to curve. Due to the significant difference between the surface area perpendicular (b_y) and parallel (b_x) to the hull of a USV (see figure 3), we propose this approach based on the assumption that the drag is significantly higher in the b_y axis of the USV compared to the b_x axis and is not compensated by the propulsion of the USV in the b_y axis (see figure 3). As such, the velocity gained by the vessel in the b_x axis before turning transforms into velocity perpendicular to the hull (in b_y axis), which causes the centripetal force required to turn the vehicle. Additionally, it was observed that a significant negative correlation exists between the velocity of the USV and its yaw rate due to loss of momentum from the vessel during a turn as the drag component overcomes the thrust provided by the propeller. Therefore, we introduce a negative covariance between the velocity and yaw rate of the USV to achieve sufficient dynamic performance by aiding the convergence of the filter.

For this Kalman filter, we write the state vector of the USV as

$$\mathbf{b} = [x_b \ y_b \ z_b \ \eta_b \ \dot{x}_b \ \dot{y}_b \ \dot{z}_b \ \dot{\eta}_b]^T, \quad (1)$$

where x_b, y_b, z_b are the position co-ordinates of the USV in the world frame, η_b is the heading of the USV, $\dot{x}_b, \dot{y}_b,$ and \dot{z}_b are the translational velocities in the world frame, and $\dot{\eta}_b$ is the heading rate. We then write the discrete state space model of the USV as

$$\mathbf{b}^{(k+1)} = \mathbf{A}\mathbf{b}^{(k)} + \mathbf{B}\mathbf{u}_b^{(k)} \quad (2)$$

$$\text{where } \mathbf{A} = \begin{bmatrix} 1 & 0 & 0 & 0 & dt & 0 & 0 & 0 \\ 0 & 1 & 0 & 0 & 0 & dt & 0 & 0 \\ 0 & 0 & 1 & 0 & 0 & 0 & dt & 0 \\ 0 & 0 & 0 & 1 & 0 & 0 & 0 & dt \\ 0 & 0 & 0 & 0 & 1 & 0 & 0 & 0 \\ 0 & 0 & 0 & 0 & 0 & 1 & 0 & 0 \\ 0 & 0 & 0 & 0 & 0 & 0 & 1 & 0 \\ 0 & 0 & 0 & 0 & 0 & 0 & 0 & 1 \end{bmatrix}, \quad (3)$$

$$\mathbf{B} = \begin{bmatrix} 0 & 0 & 0 & 0 & dt & 0 & 0 & 0 \\ 0 & 0 & 0 & 0 & 0 & dt & 0 & 0 \end{bmatrix}^T, \text{ and}$$

$$\mathbf{u}_b = \begin{bmatrix} a_x \\ a_y \end{bmatrix}.$$

Here, dt is the sampling time of the sensor, k is the discrete instance of time where $t = k \cdot dt$, a_x and a_y are the accelerations produced by drag force acting on the USV in the world frame. Since we do not have access to acceleration states, we generate an artificial input, by writing the drag force of a body with an asymmetric projected area, in its own frame, as

$$\mathbf{F}_d = m \begin{bmatrix} a_x \\ a_y \end{bmatrix}_b = - \begin{bmatrix} K_x & 0 \\ 0 & K_y \end{bmatrix} \begin{bmatrix} \dot{x}_b \\ \dot{y}_b \end{bmatrix}_b \quad (4)$$

where m is the mass of the USV, $[\bullet]_b$ denotes the vector in the body frame, and $K_x \geq 0$ and $K_y \geq 0$ are the tunable drag coefficients in the x and y axes of the USV frame respectively. For the purpose of our model, we assume that the USV has sufficient propulsion to counteract the drag in the b_x axis so as to maintain a constant velocity along its hull, and therefore, we set $K_x = 0$. We also assume low pitch and roll angles on the USV such that we can write a frame transform as

$${}^b\mathbf{R}_w = \begin{bmatrix} \cos \eta_b & \sin \eta_b \\ -\sin \eta_b & \cos \eta_b \end{bmatrix}, \quad {}^w\mathbf{R}_b = {}^b\mathbf{R}_w^T, \quad (5)$$

where ${}^w\mathbf{R}_b$ and ${}^b\mathbf{R}_w$ are rotation matrices for rotation transformation from the body frame to the world frame and vice-versa. Hence, we write the input to the system as a function of the velocity of the USV such that

$$m \begin{bmatrix} a_x \\ a_y \end{bmatrix}_w = {}^w\mathbf{R}_b \begin{bmatrix} 0.0 & 0.0 \\ 0.0 & -K_y \end{bmatrix} {}^b\mathbf{R}_w \begin{bmatrix} \dot{x} \\ \dot{y} \end{bmatrix}_w, \quad (6)$$

where $[\bullet]_w$ denotes the vector in the world frame. We then write the covariance matrix to account for the covariance between velocity and heading rate of the USV such that

$$\mathbf{Q}_b = \begin{bmatrix} \sigma_x & 0 & 0 & 0 & 0 & 0 & 0 & 0 \\ 0 & \sigma_y & 0 & 0 & 0 & 0 & 0 & 0 \\ 0 & 0 & \sigma_z & 0 & 0 & 0 & 0 & 0 \\ 0 & 0 & 0 & \sigma_\eta & 0 & 0 & 0 & 0 \\ 0 & 0 & 0 & 0 & \sigma_{\dot{x}} & 0 & 0 & \sigma_{\dot{x}\dot{\eta}} \\ 0 & 0 & 0 & 0 & 0 & \sigma_{\dot{y}} & 0 & \sigma_{\dot{y}\dot{\eta}} \\ 0 & 0 & 0 & 0 & 0 & 0 & \sigma_z & 0 \\ 0 & 0 & 0 & 0 & \sigma_{\dot{x}\dot{\eta}} & \sigma_{\dot{y}\dot{\eta}} & 0 & \sigma_{\dot{\eta}} \end{bmatrix}. \quad (7)$$

Since a USV experiences a significant reduction in its lateral velocity during a turn, we set $\sigma_{\dot{x}\dot{\eta}}, \sigma_{\dot{y}\dot{\eta}}, \sigma_{\dot{x}\dot{\eta}}, \sigma_{\dot{y}\dot{\eta}} < 0$ to reflect this negative co-relation. These tunable parameters improve the prediction performance in the turns, and depend on the design/dimensions of the USV (-0.3 for our setup).

B. UAV Prediction and Control Model

The UAV prediction model used in the proposed MPC is based on the Euler approximation of single particle kinematics in the world frame, and is identical to our previous work [6]. We employ the following discrete linear time-invariant system:

$$\mathbf{x}^{(k+1)} = \mathbf{D}\mathbf{x}^{(k)} + \mathbf{E}\mathbf{u}_d^{(k)}, \text{ where} \quad (8)$$

$$\mathbf{x} = \begin{bmatrix} x_d & \dot{x}_d & \ddot{x}_d & y_d & \dot{y}_d & \ddot{y}_d \\ z_d & \dot{z}_d & \ddot{z}_d & \psi_d & \dot{\psi}_d & \ddot{\psi}_d \end{bmatrix}^T, \quad (9)$$

$$\text{and } \mathbf{u}_d^{(k)} = \begin{bmatrix} \dot{x}_d & \dot{y}_d & \dot{z}_d & \dot{\psi}_d \end{bmatrix}^T. \quad (10)$$

Here x_d, y_d, z_d are the position co-ordinates of the UAV, ψ_d is the heading of the UAV, and their subsequent derivatives form the state vector \mathbf{x} and the input vector \mathbf{u}_d . For this model (8), the state matrix \mathbf{D} and the input matrix \mathbf{E} can be described through the Kronecker product (\otimes), such that

$$\mathbf{D}_{12 \times 12} = \mathbf{I}_{4 \times 4} \otimes \mathbf{D}'_{3 \times 3}, \text{ where } \mathbf{D}' = \begin{bmatrix} 1 & \Delta t_p & \frac{\Delta t_p^2}{2} \\ 0 & 1 & \Delta t_p \\ 0 & 0 & 1 \end{bmatrix}, \quad (11)$$

$$\mathbf{E}_{12 \times 4} = \mathbf{I}_{4 \times 4} \otimes \mathbf{E}'_{3 \times 1}, \text{ where } \mathbf{E}' = \begin{bmatrix} \frac{\Delta t_p^3}{6} & \frac{\Delta t_p^2}{2} & \Delta t_p \end{bmatrix}^T, \quad (12)$$

where \mathbf{I} is an identity matrix, and $\Delta t_p = 0.01$ seconds. We use these UAV and USV prediction models inside a MPC-based control approach similar to our previous work [6]. However, owing to the expanded prediction capability, we modify the cost function to include predicted translation velocities which leads to a decrease in average tracking error. The cost function is then defined as

$$\min_{\mathbf{u}_{d1}, \dots, \mathbf{u}_{dM_c}} J(\mathbf{x}, \mathbf{u}_d) = \underbrace{\sum_{m=1}^{M_p} \tilde{\mathbf{x}}_m^T \mathbf{S} \tilde{\mathbf{x}}_m + \mathbf{h}_m^T \mathbf{T} \mathbf{h}_m}_{J_1} + \underbrace{\sum_{m=1}^{M_p} \alpha_L f(\tilde{z}_m) (\dot{z}_b - \dot{z}_d)^2}_{J_2},$$

subject to :

$$\begin{aligned} \tilde{\mathbf{x}}_m &= \tilde{\mathbf{x}}_m^* - \mathbf{x}_m, \\ \tilde{z}_m &= \tilde{z}_m^* - z_m, \\ \mathbf{h}_m &= \mathbf{u}_{d_m} - \mathbf{u}_{d_{m-1}}, \\ \mathbf{x}_{m+1} &= \mathbf{D}\mathbf{x}_m + \mathbf{E}\mathbf{u}_{d_m} \quad \forall m \leq M_c, \\ \mathbf{x}_{m+1} &= \mathbf{D}\mathbf{x}_m + \mathbf{E}\mathbf{u}_{d_{M_c}} \quad \forall m > M_c, \\ \mathbf{u}_{d_{min}} &\leq \mathbf{u}_{d_m} \leq \mathbf{u}_{d_{max}}, \\ \mathbf{x}_0 &= \mathbf{x}_{initial}, \\ \mathbf{u}_{d0} &= \mathbf{u}_{d_{initial}}, \\ &\forall \{m : m \in \mathbb{N}, 1 \leq m \leq M_p\}, \end{aligned} \quad (13)$$

where $\tilde{\mathbf{x}}_m^*$ is the desired state, $\tilde{\mathbf{x}}_m$ is the error vector, \tilde{z}_m is the error in z_m position, \mathbf{h}_m is the rate of control input change to ensure smooth input to the UAV, $M_p (= 100)$ is the prediction horizon, and $M_c (= 40)$ is the control horizon. \mathbf{S} and \mathbf{T} are the corresponding penalty matrices with configurable weights for performance tuning, while $\alpha_L (= 1200)$ is the scalar for tuning J_2 . The cost function is divided into two parts i.e. J_1 and J_2 , and while J_1 remains active at all times, J_2 is activated by the sigmoid function in the vicinity of the landing deck to control the relative velocity (as opposed to controlling relative tilt in

[6]) between the UAV and the USV. The sigmoid function is defined as

$$f(\tilde{z}_m) = \begin{cases} \left(1.0 + \exp\left(\frac{-\tilde{z}_m - h_d}{-0.15}\right)\right)^{-1}, & \text{if } \tilde{z}_m \geq 0.16 \\ \left(1.0 + \exp\left(\frac{\tilde{z}_m - 0.1}{-0.01}\right)\right)^{-1}, & \text{otherwise,} \end{cases} \quad (14)$$

where $h_d (= 1.1)$ controls the waiting region during a landing attempt.

IV. SIMULATION EXPERIMENTS

We present our results through comparison with the state-of-the-art, presented in [18], to highlight the advantages of our proposed approach. For clarity, we present this comparison in two separate sections; first for trajectory predictions, and second for chasing and landing. For these comparisons, the two types of models presented in [18] will be labelled as ‘3D UKF’ and ‘12D LKF’. The former stands for the complex UKF model with hydrodynamic and hydrostatic forces, and the latter stands for the simplified point-mass kinematics model. For ‘3D UKF’ and ‘12D LKF’, we use four sensory inputs comprising of two visual pose estimation methods (UltraViolet Direction And Ranging (UVDAR) system [21] and AprilTag [22]) as well as two communication-reliant sensors (Global Navigation Satellite System (GNSS) and IMU). It is of note that the state-of-the-art method can also run solely on visual pose estimation with degraded performance, but we compare their best-case scenario of four sensory inputs to our bare-minimum scenario of a single input via AprilTag pose estimates. For these simulation experiments, we use the Virtual RobotX (VRX) simulation environment in Gazebo [23] to generate the motion of the USV and employ the MRS-system [20] to simulate and control the UAV. For our simulated UAV model, we use a T650 quadrotor frame weighing 3.6 kg, carrying a Garmin LiDAR for altitude measurement above the landing deck, and an Intel RealSense D435 camera for live in-simulation video. This setup closely resembles the setup used in the real-world experiments conducted for this work.

A. Trajectory Prediction Results

The USV follows an 8-figure trajectory which is specially selected such that the time spent in turning is longer than the chosen 2-second prediction window for these comparisons. For this comparison, both ‘12D LKF’ and ‘3D UKF’ are compared with our approach, which is marked as ‘CurviTrack’. Figure 4 shows the predicted paths against the ground truth measured in the simulator. Table I shows the mean error, average error, and standard deviation of the error for predictions in the xy-plane for each technique. We highlight that, for 1-second predictions, our technique provides over 70 % reduction in error compared to ‘12D LKF’ and 40 % reduction over the complex model employed in ‘12D UKF’. Similarly, our approach also offers a 7-fold decrease in standard deviation (increase in certainty) over the ‘12 LKF’ and a near 3-fold decrease in standard deviation over the ‘3D UKF’ method. We note that for our high-level MPC approach, we use a prediction horizon of 1 s. However, predictions up to $t = 2.0$ s become important for

t	Method	Mean (m)	Max (m)	Std. Dev. (m)
1.0 s	12D LKF	1.71	4.01	1.31
	3D UKF	0.79	2.03	0.51
	CurviTrack	0.48	0.95	0.18
2.0 s	12D LKF	2.56	5.92	1.97
	3D UKF	1.28	3.35	0.89
	CurviTrack	0.90	1.66	0.34

TABLE I: Mean error, maximum error, and standard deviation of the error for predictions in comparison to ‘12D LKF’ and ‘3D UKF’ in [18].

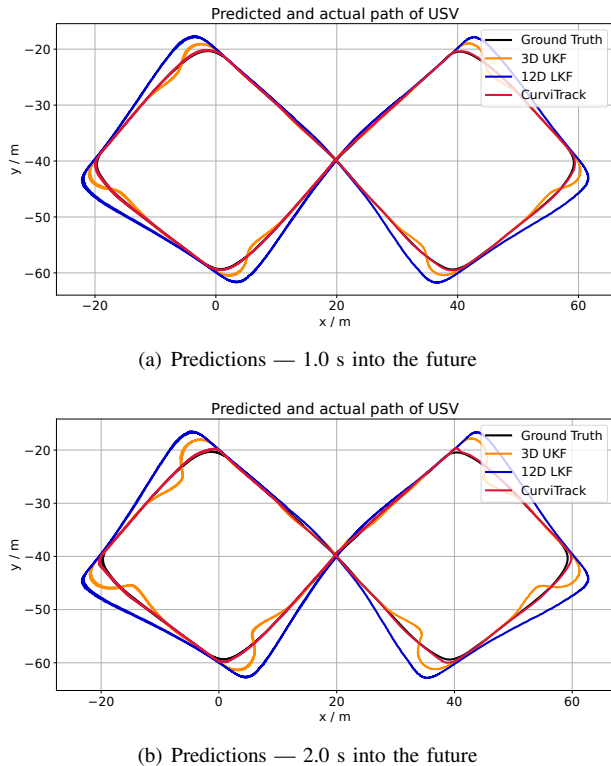


Fig. 4: Comparison between predictions made by our proposed approach and the state-of-the-art approach by Novák et al. [18].

many high-level cascaded control policies, which are compute-limited, and therefore, choose to run at a much slower rate than low-level controllers. For those scenarios, our proposed method offers near 65% reduction and near 30% reduction in mean error compared to ‘12D LKF’ and ‘3D UKF’ as shown in Table I. Hence, for predictions, our efficient curvilinear model outperforms the state-of-the-art by a significant margin without using communication and, therefore, without multimodal sensory input.

B. Chasing and Landing Results

For tracking and landing, we select ‘12D LKF’ for our comparison as a majority of aforementioned literature uses linear predictions for landings performed on moving USVs, and so, we highlight the advantages of switching to our curvilinear approach. We perform the comparison over a special triangular trajectory (figure 5), designed to push the

limits of the proposed approach by using harsh 120° turns which are uncommon for real-missions for sweeping an area. The trajectory is also specifically designed such that the USV spends an equal amount of time moving in a straight line and moving in a curved path. The predictions for both estimators are sent to the MPC, which controls the UAV to follow the USV around the trajectory.

For tracking, we present our results through figure 6 which summarises the horizontal distance between the UAV and the USV during the turns ($\eta_b > 0.1 \text{ rad s}^{-1}$), where, it can be seen that our proposed approach doubles the instances where tracking distance is within 0.5 m of the USV throughout the trajectory. It is also to be noted that our approach allows the UAV to be within 1.0 m of the USV in nearly 80% of the instances. The median follow distance of our proposed approach (0.67 m) is found to be 30% lower than the compared approach (0.97 m). It is important to note that not only does our approach yield a direct improvement in the tracking performance compared to a linear approach, this improvement of performance in 0.5 m distance is approximately the width of our UAV which significantly increases the probability of a successful landing, as highlighted in the next section.

We ran a statistical analysis of multiple attempted landings on the USV deck in the simulation during the triangular trajectory tracking. Once the UAV was following the USV, the mission controller initiated landing at a randomly chosen time, and a landing attempt was logged. A landing attempt was considered successful if the UAV was within a radius of 1.0 m from the centre of the landing deck and its altitude was within 0.15 m from the landing deck (such that the landing gear touched the deck). The experimental setup prevents landing in low confidence and, thus, prevents either of the approaches from landing outside the deck. Instead, landings are aborted, and UAV regains altitude if the visual marker of the USV cannot be seen for more than 0.5 s. We compare the successful landings against the aborted landings to represent the time saved from aborting and retrying landing during time-constrained missions. When compared against the ‘12D LKF’, our approach succeeded in landing 25 times out of 50 attempts (50%), whereas the linear approach succeeded only 18 times out of 50 attempts (36.0%). When compared against the ‘12D LKF’, our approach showed 40% increase in successful landing instances for all the simulated landing attempts, even for an aggressively curving trajectory shown. This clearly highlights the aforementioned need to predict curvilinear motion and save time for autonomous missions. We emphasise that while this particular triangular trajectory allots equal time to linear and curvilinear motion, for a trajectory with a higher number of turns (as is common for search patterns in marine environments), we expect the performance of our approach to stand out significantly more than it does in this comparison. We achieve this performance gain for a harsh and unrealistic turn angle in the trajectory, which pushes the limits of the tracking methodology.

V. REAL-WORLD EXPERIMENTS

In addition to the simulation environment, we present the results of our approach in two real-world conditions which

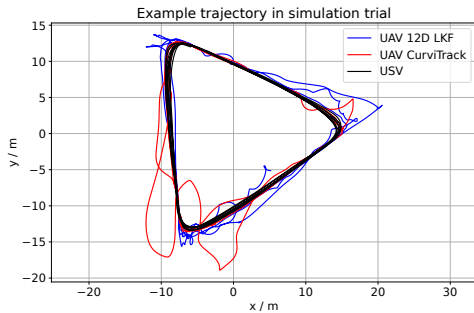


Fig. 5: A randomly picked example triangle trajectory for comparative analysis. Visible deviations arise from the search phase performed after aborted landings.

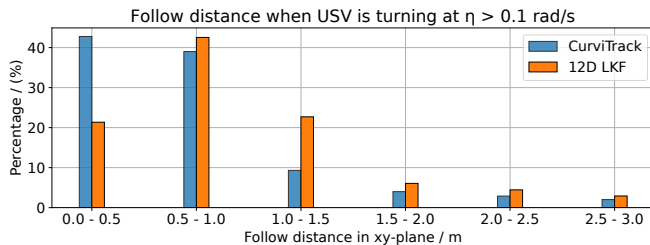


Fig. 6: Statistical analysis on tracking error between our 'CurviTrack' and '12D LKF' model in simulation for a triangular trajectory when USV is turning at a $\eta_b > 0.1 \text{ rad s}^{-1}$.

cover both land and water to thoroughly test the robustness of our proposed method in adverse conditions. For our real-world flights, we employed a 4.5 kg T650 quadrotor equipped with vertical pontoons [24] for emergency landing over water (see figure 1). In addition, the sensor stack included a Garmin LiDAR for laser-ranging of altitude above the landing deck, a Basler camera for the live video feed, and an Intel NUC for onboard real-time processing of the algorithms, data, and video. To validate our approach, we rigorously test our method in two very different environments to push the limits of estimation and tracking capabilities, and to demonstrate robustness.

For the first set of experiments, we test the predictions over land in a high-speed chase of up to 5 m s^{-1} (the USV moves two body-lengths every second, and UAV moves five body-lengths every second) where the algorithm is challenged by a rapidly curving path over land with unpredictable input from a human operator. For this experiment, we approximate the moving USV using a wooden board with an AprilTag [22] affixed on top, and this board is dragged on the ground by the operator. These experiments present the robustness of our method as the operator can change the magnitude and direction of velocity at their wish and produce turns that are infeasible and unexpected in the marine environment for UAV-USV missions. For example, the assumption of drag in the y-axis is deliberately broken by inducing a side slip in the platform while dragging. For these land-based experiments, we highlight our prediction and tracking performance.

For the second set of experiments, two different kinds of USVs were tested in fresh-water environment to confirm the

adaptability of the proposed approach to vessels of different sizes. For the first scenario, an inflatable dinghy is towed behind a paddle-driven boat to represent a low-speed (up to 2 m s^{-1}) high-drag marine vessel with a 2m by 2m landing deck (figure 1). For the second scenario, a sub-5m autonomous USV, capable of moving at speeds of up to 3 m s^{-1} , was used to represent a realistic watercraft deployed for missions in fresh-water environments (figure 1). For these fresh-water experiments, we present our prediction, tracking, and landing capabilities.

A. Trajectory Prediction Results

As seen through figure 7, the prediction method is robust to quick changes in direction and manages to accurately predict the future for both land-based and water-based experiments. In the land-based experiments, unlike the simulation environment, rapid changes are made in the direction of motion

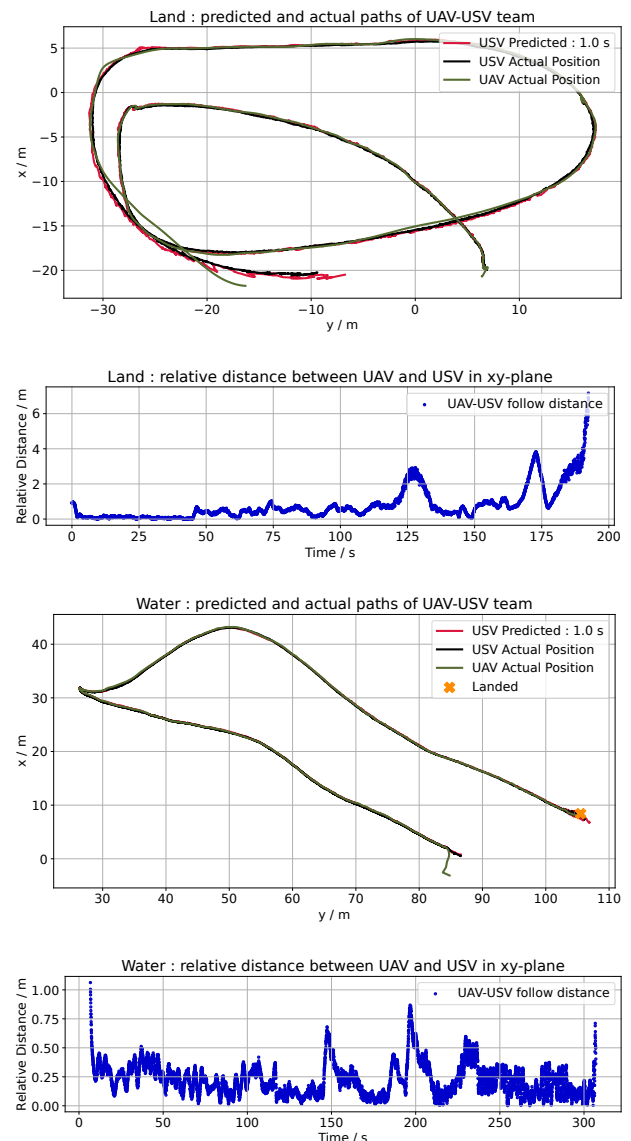


Fig. 7: Predictions and relative distance for chase during land-based and water-based real-world experiments.

by the operator. The only negative impact appears to be the irregularity of the predicted trajectory, which arises from a continuous side slip, causing the projected motion to curve more aggressively than the ground-truth. However, as evident from the figure, the UAV is able to follow the predictions on the curved paths without losing track. As seen in figure 7, when the operator crosses the maximum allowed horizontal acceleration/deceleration of the mission, the UAV lags behind but quickly recovers without losing track of the USV.

In the fresh-water environment, the predictions are smoother than in land-based experiments due to the uniform drag experienced as per the internal model, and consequently, the predictions line up perfectly with the path taken by the marine vessel.

These experimental runs strongly support the ability of the proposed approach to make reliable predictions about the future of the USV during curvilinear trajectories in real-world scenarios.

B. Chasing and Landing Results

As shown in figure 7, the UAV is able to follow the landing target closely throughout the turns and is able to land on the USV after tracking it through the curvilinear trajectory. These experiments can also be seen in the media attached with the paper and further prove the robustness of our approach to the changes in the environment as well as applicability to real UAVs and USVs of different sizes.

VI. CONCLUSION

In this work, we presented a novel approach for the autonomous landing of UAVs onto various moving USV in marine environments for following high-speed curvilinear trajectories. Our proposed decentralized solution leverages visual pose estimation and an efficient motion model for predicting and tracking the moving USV, enabling precise and robust landing manoeuvres. Through statistical analysis in simulation experiments and various real-world experiments, we have demonstrated a decrease in prediction error and an increase in tracking and landing performance for our novel method in comparison to the state-of-the-art. This real-time onboard model can converge and predict for any sensor setup with robust pose estimation without requiring communication.

REFERENCES

- [1] R. R. Murphy, E. Steimle, C. Griffin, C. Cullins, M. Hall, and K. Pratt, "Cooperative use of unmanned sea surface and micro aerial vehicles at hurricane wilma," *Journal of Field Robotics*, vol. 25, no. 3, pp. 164–180, 2008.
- [2] M. Lindemuth, R. Murphy, E. Steimle, W. Armitage, K. Dreger, T. Elliot, M. Hall, D. Kalyadin, J. Kramer, M. Palankar, K. Pratt, and C. Griffin, "Sea robot-assisted inspection," *IEEE Robotics & Automation Magazine*, vol. 18, no. 2, pp. 96–107, 2011.
- [3] F. F. Ramírez, D. S. Benitez, E. B. Portas, and J. A. L. Orozco, "Coordinated sea rescue system based on unmanned air vehicles and surface vessels," in *OCEANS 2011 IEEE - Spain*, 2011, pp. 1–10.
- [4] J. M. Riola, J. J. Diaz, and J. M. Giron-Sierra, "The prediction of calm opportunities for landing on a ship: Aspects of the problem," in *OCEANS 2011 IEEE - Spain*, 2011, pp. 1–8.
- [5] S. Küchler, T. Mahl, J. Neupert, K. Schneider, and O. Sawodny, "Active control for an offshore crane using prediction of the vessel's motion," *IEEE/ASME Transactions on Mechatronics*, vol. 16, no. 2, pp. 297–309, 2011.
- [6] P. M. Gupta, E. Pairet, T. Nascimento, and M. Saska, "Landing a uav in harsh winds and turbulent open waters," *IEEE Robotics and Automation Letters*, vol. 8, no. 2, pp. 744–751, 2023.
- [7] J. Li, G. Zhang, C. Jiang, and W. Zhang, "A survey of maritime unmanned search system: Theory, applications and future directions," *Ocean Engineering*, vol. 285, p. 115359, 2023.
- [8] R. Polvara, S. Sharma, J. Wan, A. Manning, and R. Sutton, "Vision-based autonomous landing of a quadrotor on the perturbed deck of an unmanned surface vehicle," *Drones*, vol. 2, no. 2, 2018.
- [9] S. Abujoub, J. McPhee, C. Westin, and R. A. Irani, "Unmanned aerial vehicle landing on maritime vessels using signal prediction of the ship motion," in *OCEANS 2018 MTS/IEEE Charleston*, 2018, pp. 1–9.
- [10] L. Yang, Z. Liu, X. Wang, G. Wang, X. Hu, and Y. Xi, "Autonomous landing of a rotor unmanned aerial vehicle on a boat using image-based visual servoing," in *2021 IEEE International Conference on Robotics and Biomimetics (ROBIO)*, 2021, pp. 1848–1854.
- [11] B. Herissé, T. Hamel, R. Mahony, and F.-X. Russotto, "Landing a vtol unmanned aerial vehicle on a moving platform using optical flow," *IEEE Transactions on Robotics*, vol. 28, no. 1, pp. 77–89, 2012.
- [12] S. K. Cengiz and L. Ucun, "Optimal controller design for autonomous quadrotor landing on moving platform," *Simulation Modelling Practice and Theory*, vol. 119, p. 102565, 2022.
- [13] Z. Zhao, P. Han, Y. Xu, W. Xie, W. Zhang, K. Liang, and Q. Zeng, "Vision-based autonomous landing control of a multi-rotor aerial vehicle on a moving platform with experimental validations," *IFAC-PapersOnLine*, vol. 55, no. 3, pp. 1–6, 2022, 16th IFAC Symposium on Large Scale Complex Systems: Theory and Applications LSS 2022.
- [14] D. Falanga, A. Zanchettin, A. Simovic, J. Delmerico, and D. Scaramuzza, "Vision-based autonomous quadrotor landing on a moving platform," in *2017 IEEE International Symposium on Safety, Security and Rescue Robotics (SSRR)*, 2017, pp. 200–207.
- [15] A. Borowczyk, D.-T. Nguyen, A. P.-V. Nguyen, D. Q. Nguyen, D. Saussié, and J. Le Ny, "Autonomous landing of a quadcopter on a high-speed ground vehicle," *Journal of Guidance, Control, and Dynamics*, vol. 40, no. 9, pp. 2378–2385, 2017.
- [16] B. Lee, V. Saj, M. Benedict, and D. Kalathil, "A vision-based control method for autonomous landing of vertical flight aircraft on a moving platform without using gps," 2020.
- [17] T. Baca, P. Stepan, and M. Saska, "Autonomous landing on a moving car with unmanned aerial vehicle," in *2017 European Conference on Mobile Robots (ECMR)*, 2017, pp. 1–6.
- [18] F. Novák, T. Báča, O. Procházka, and M. Saska, "State estimation of marine vessels affected by waves by unmanned aerial vehicles," *Ocean Engineering*, vol. 323, p. 120606, 2025.
- [19] O. Procházka, F. Novák, T. Báča, P. M. Gupta, R. Pěnička, and M. Saska, "Model predictive control-based trajectory generation for agile landing of unmanned aerial vehicle on a moving boat," p. 119164, 2024.
- [20] T. Baca, M. Petrlik, M. Vrba, V. Spurny, R. Penicka, D. Hert, and M. Saska, "The MRS UAV System: Pushing the Frontiers of Reproducible Research, Real-world Deployment, and Education with Autonomous Unmanned Aerial Vehicles," *Journal of Intelligent & Robotic Systems*, vol. 102, no. 26, pp. 1–28, May 2021.
- [21] V. Walter, N. Staub, A. Franchi, and M. Saska, "Uvdar system for visual relative localization with application to leader-follower formations of multirotor uavs," *IEEE Robotics and Automation Letters*, vol. 4, no. 3, pp. 2637–2644, 2019.
- [22] J. Wang and E. Olson, "Apriltag 2: Efficient and robust fiducial detection," in *2016 IEEE/RSJ International Conference on Intelligent Robots and Systems (IROS)*, 2016, pp. 4193–4198.
- [23] B. Bingham, C. Agüero, M. McCarrin, J. Klamo, J. Malia, K. Allen, T. Lum, M. Rawson, and R. Waqar, "Toward maritime robotic simulation in gazebo," in *OCEANS 2019 MTS/IEEE SEATTLE*, 2019, pp. 1–10.
- [24] D. Hert, T. Baca, P. Petracek, V. Kratyk, V. Spurny, M. Petrlik, M. Vrba, D. Zaitlik, P. Stoudek, V. Walter, P. Stepan, J. Horyna, V. Pritzl, G. Silano, D. Bonilla Licea, P. Stübinger, R. Penicka, T. Nascimento, and M. Saska, "Mrs modular uav hardware platforms for supporting research in real-world outdoor and indoor environments," in *2022 International Conference on Unmanned Aircraft Systems (ICUAS)*, 2022, pp. 1264–1273.